Corrigendum: Data-driven and learning-based interpolations of along-track Nadir and wide-swath SWOT altimetry observations

MAXIME BEAUCHAMP, IMT Atlantique Bretagne-Pays de la Loire, France
RONAN FABLET, IMT Atlantique Bretagne-Pays de la Loire, France
CLÉMENT UBELMANN, Ocean Next, France
MAXIME BALLAROTTA, Collecte Localisation Satellites (CLS), France
BERTRAND CHAPRON, IFREMER, France

We detected an error in the datasets used for testing the FP-GENN/ConvAE algorithms in the paper. The other algorithms used in the paper (OI, AnDA, VE-DINEOF) are not affected. We precise that the FP-GENN/ConvAE algorithms remains strictly identical but the datasets used with this algorithm oversampled the observations with a factor of 5, leading to an overestimation of the FP-GENN/ConvAE performances. Hopefully, the scientific conclusions remains unaffected: as already stated in the previous version, FP-GENN is still the best algorithm among all the methods tested in the paper but we had to produce a new set of results taking into account this correction. We updated the Figures and qualified a bit some of the comments and conclusions in this corrigendum accordingly.

1 NEW SETUP OF THE NN-BASED ALGORITHMS

In the previous work of [2] over the Mediterranean sea, using an along-track data aggregation of $t_k \pm d$ days over a specific day t_k helps to improve the performance for AnDA. In the first version of the paper, and because of the bug in the dataset used for FP-GENN/ConvAE, it was also the case and an aggregation of ±5 days was used. After correction, it is no longer the case, neither for AnDA nor for neural-based methods. As a consequence, all the methods now use value of $d = 0$. Figure 1 gives an example on August 4, 2013 of the two types of datasets used in this work (along-track nadir with/without wide-swath pseudo-observations).

Authors' addresses: Maxime Beauchamp, maxime.beauchamp@imt-atlantique.fr, IMT Atlantique Bretagne-Pays de la Loire, Brest, France; Ronan Fablet, IMT Atlantique Bretagne-Pays de la Loire, Brest, France; Clément Ubelmann, Ocean Next, Grenoble, France; Maxime Ballarotta, Collecte Localisation Satellites (CLS), Ramonville St-Agne, France; Bertrand Chapron, IFREMER, Plouzané, France.

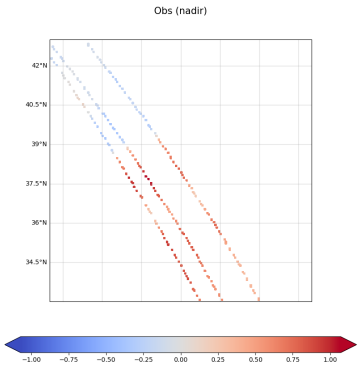

(a) nadir (d=0)

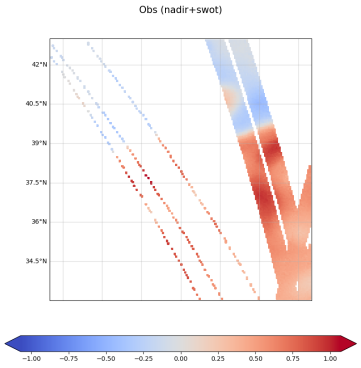

(b) nadir (d=0) + swot

Fig. 1. along-track nadir and wide-swath pseudo-observations for August 4, 2013

Next, using a 0-day aggregation of the along-track nadir data also influences the best configuration of the NN-based interpolators. If the unsupervised strategy often led to the best performance in the previous version, it is now the supervised strategy that behaves best: the inputs are the observations involving high missing data rates and the targets are the gap-free NATL60 data. The DUACS OI product is also used as a covariate in the inputs, because we think that this may give a prior information about how the anomaly field $d\mathbf{x}$ is distributed.

According to this new FP-GENN/ConvAE setup, we provide in Section 2 an updated version of Figures 2, 3 and Table 1 with the corrected statistics corresponding to the FP-GENN/ConvAE algorithms.

2 EVALUATION

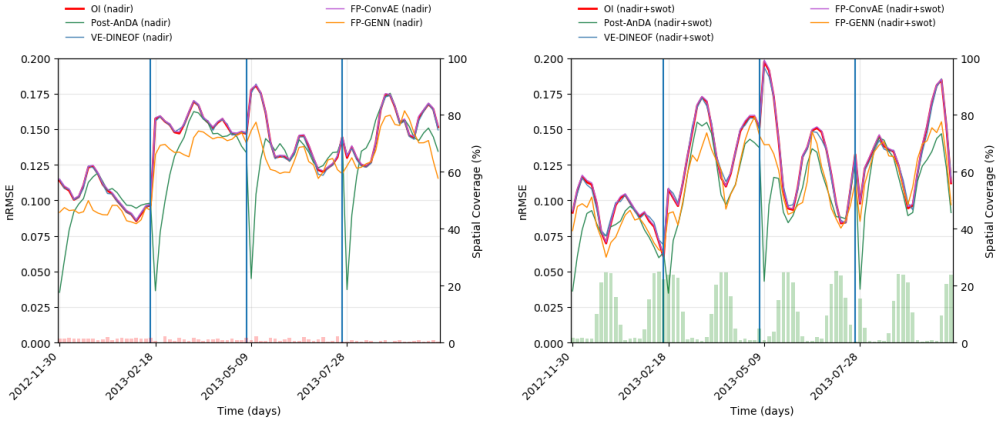

(a) nadir (b) nadir+swot

Fig. 2. Daily spatial nRMSE computed on the 80-days non-continuous validation period for OI, (post-)AnDA, VE-DINEOF, FP-ConvAE and FP-GENN. The spatial coverage of 0-days accumulated along-track nadir and wide-swath SWOT data are respectively provided by the red and green-colored barplots

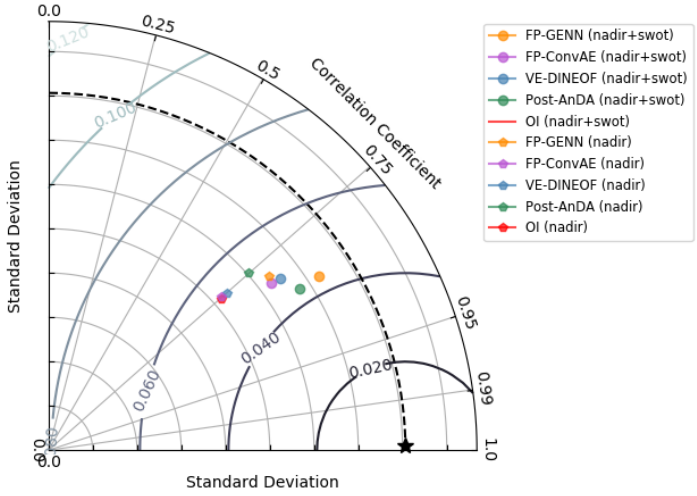

Fig. 3. Taylor diagram computed on the 80-days non-continuous validation period for OI, (post-)AnDA, VE-DINEOF, FP-ConvAE and FP-GENN

	Model type	median	$q_{0.5}$	$q_{0.95}$
nadir	OI	0.14	0.10	0.17
	AnDA	0.14	0.10	0.17
	VE-DINEOF	0.14	0.10	0.17
	FP-ConvAE	0.14	0.10	0.18
	FP-GENN	**0.13**	**0.09**	**0.16**
nadir + SWOT	OI	0.12	0.08	0.17
	AnDA	0.11	0.08	0.15
	VE-DINEOF	0.12	0.09	0.17
	FP-ConvAE	0.12	0.09	0.16
	FP-GENN	**0.11**	**0.07**	**0.15**

	Model type	median	$q_{0.5}$	$q_{0.95}$
nadir	∇_{OI}	0.52	0.40	0.64
	∇_{AnDA}	0.52	**0.40**	**0.63**
	$\nabla_{\mathrm{VE-DINEOF}}$	0.53	0.41	0.65
	$\nabla_{\mathrm{FP-ConvAE}}$	0.54	0.42	0.66
	$\nabla_{\mathrm{FP-GENN}}$	**0.52**	0.41	0.64
nadir + SWOT	∇_{OI}	0.49	0.35	0.66
	∇_{AnDA}	**0.45**	**0.32**	0.63
	$\nabla_{\mathrm{VE-DINEOF}}$	0.52	0.40	0.67
	$\nabla_{\mathrm{FP-ConvAE}}$	0.51	0.36	0.68
	$\nabla_{\mathrm{FP-GENN}}$	0.48	0.36	**0.45**

Table 1. Daily SSH and SSH gradient field median nRMSE and associated 5th and 95th percentile computed using the 4×10 days at the center of the 4 validation periods for OI, (post-)AnDA, VE-DINEOF, FP-ConvAE and FP-GENN for both nadir use only and joint assimilation/learning with wide-swath SWOT data

The conclusions remain unchanged even if the performance of FP-GENN is lower than initially described in the first version of the paper. This is also the case when computing the radially averaged power spectra as a spatial domain averaged over the 80-days validation period and the associated signal-to-noise ratio for joint use of along-track nadir with SWOT data (not shown here): we now observe that AnDA lead to a better constraint of the SSH spectrum compared to the actual OI capabilities. It produces a spectrum closer to the ground truth real spectrum, by catching up the submesoscale range up to 70km (when picking up signal-to-noise ratio equals to 0.5) when considering a joint learning from along-track nadir and additional wide-swath SWOT data. It does not seem to be the case for FP-GENN, but this should be possible to improve this results by improving the fixed-point solver of the algorithm and using a gradient-based version inspired by 4DVar data assimilation [1].

Last, we also provide the updated versions of both SSH and gradient field reconstructions with updated version of FP-GENN/ConvAE on August 4, 2013:

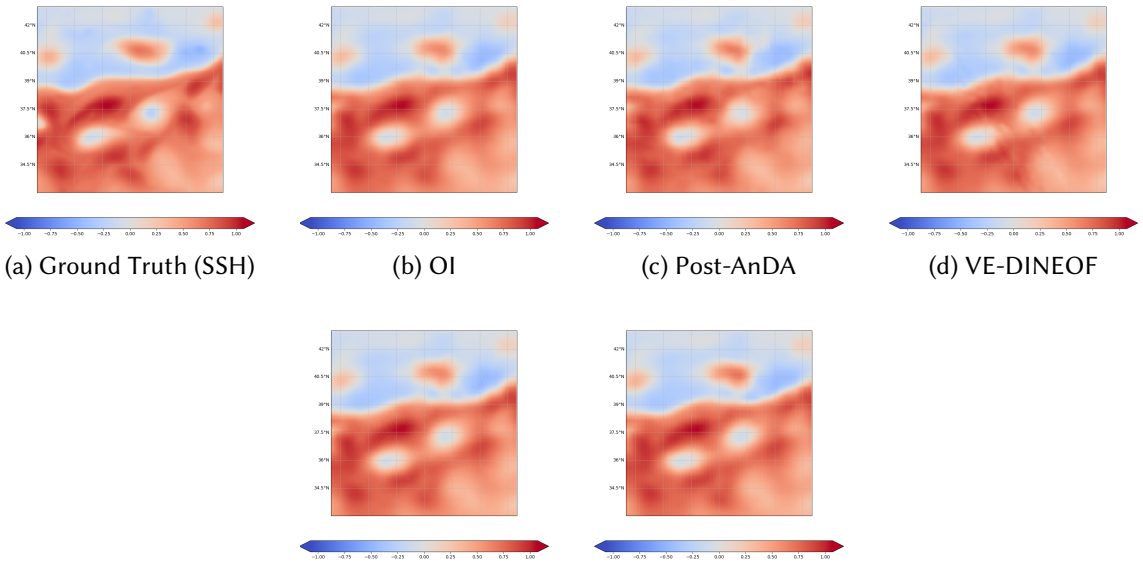

(a) Ground Truth (SSH) (b) OI (c) Post-AnDA (d) VE-DINEOF

(e) FP-ConvAE (f) FP-GENN

Fig. 4. Global SSH field reconstruction (August 4, 2013) obtained by OI, (post-)AnDA, VE-DINEOF, FP-ConvAE and FP-GENN using along-track nadir data only

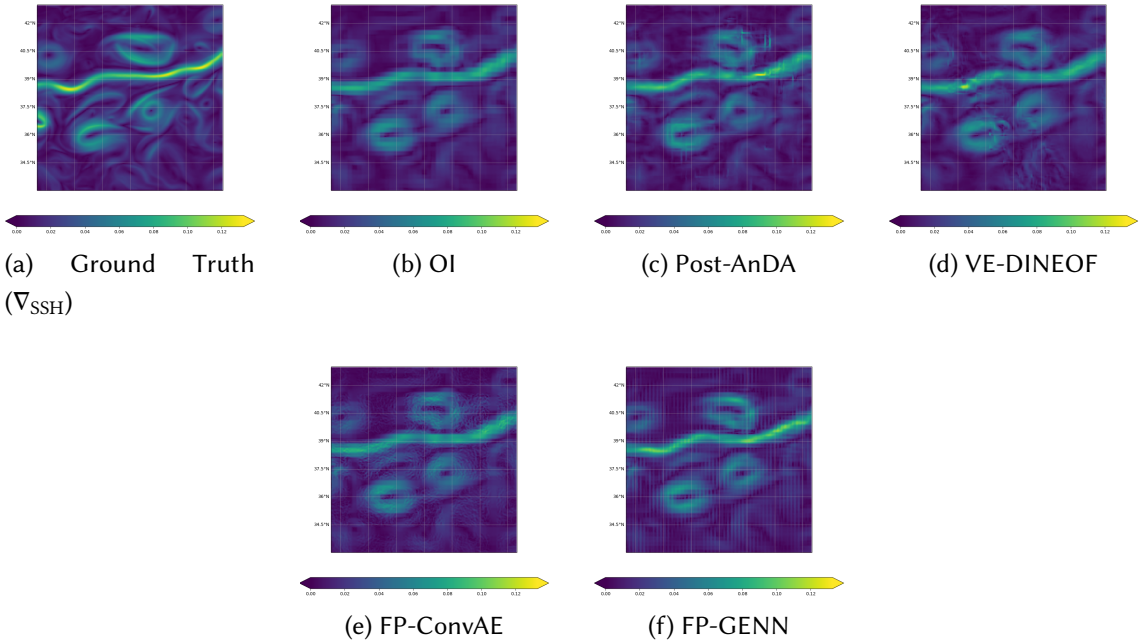

(a) Ground Truth (∇_{SSH}) (b) OI (c) Post-AnDA (d) VE-DINEOF

(e) FP-ConvAE (f) FP-GENN

Fig. 5. Global SSH gradient field reconstruction (August 4, 2013) obtained by OI, (post-)AnDA, VE-DINEOF, FP-ConvAE and FP-GENN using along-track nadir data only

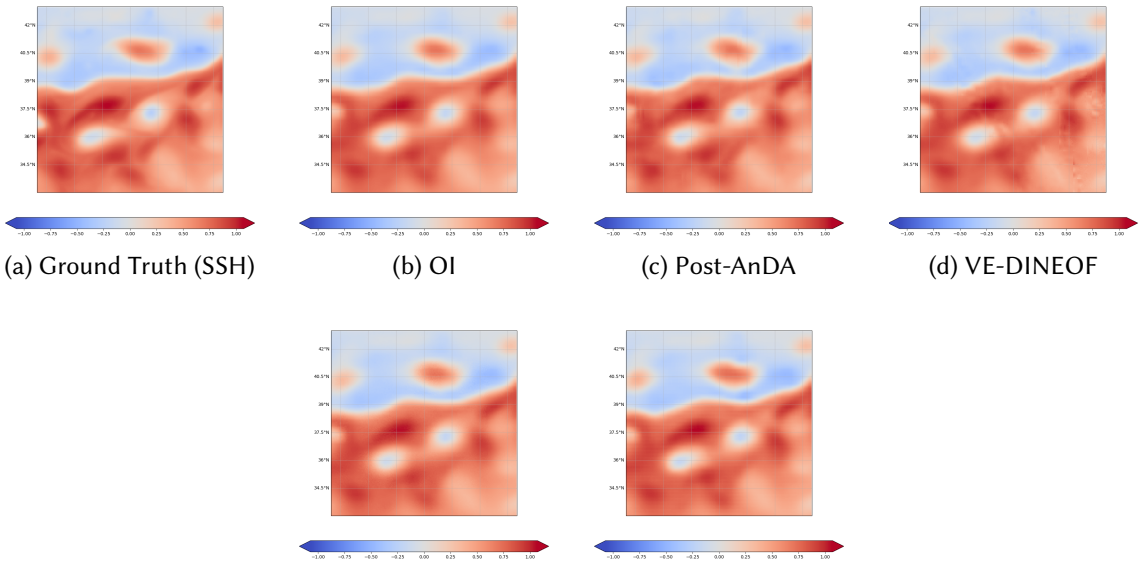

(a) Ground Truth (SSH) (b) OI (c) Post-AnDA (d) VE-DINEOF

(e) FP-ConvAE (f) FP-GENN

Fig. 6. Global SSH field reconstruction (August 4, 2013) obtained by OI, (post-)AnDA, VE-DINEOF, FP-ConvAE and FP-GENN using along-track nadir and wide-swath SWOT data

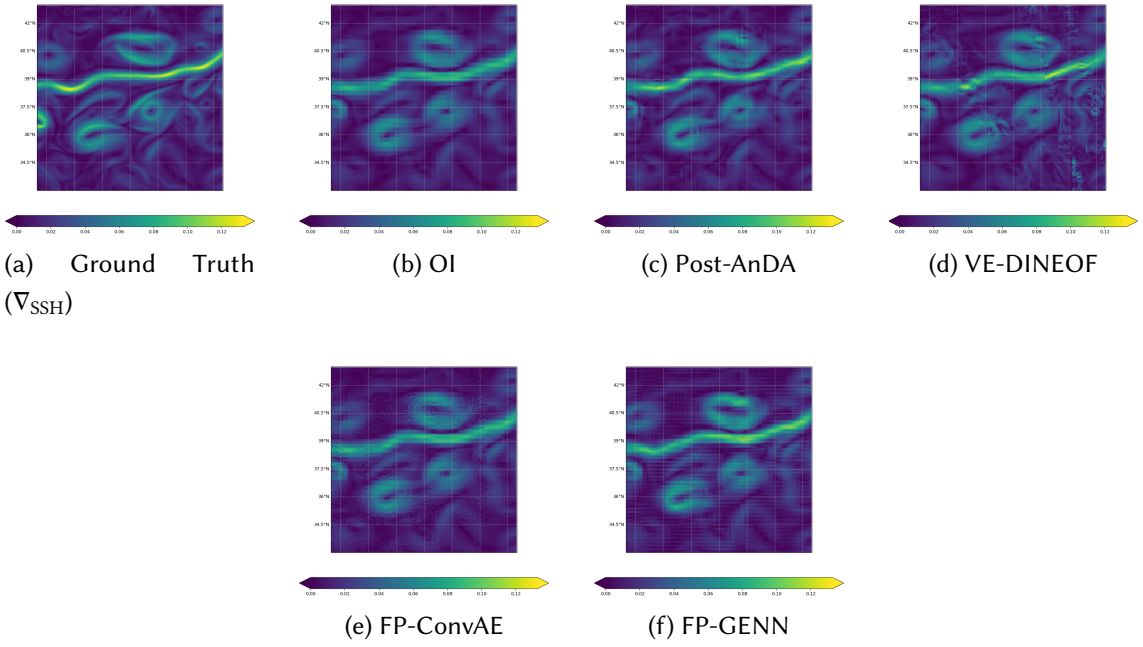

(a) Ground Truth (∇_{SSH}) (b) OI (c) Post-AnDA (d) VE-DINEOF

(e) FP-ConvAE (f) FP-GENN

Fig. 7. Global SSH gradient field reconstruction (August 4, 2013) obtained by OI, (post-)AnDA, VE-DINEOF, FP-ConvAE and FP-GENN using along-track nadir and wide-swath SWOT data

REFERENCES

[1] Ronan Fablet, Lucas Drumetz, and Francois Rousseau. 2020. Joint learning of variational representations and solvers for inverse problems with partially-observed data. (2020). arXiv:cs.LG/2006.03653

[2] M. Lopez-Radcenco, A. Pascual, L. Gomez-Navarro, A. Aissa-El-Bey, B. Chapron, and R. Fablet. 2019. Analog Data Assimilation of Along-Track Nadir and Wide-Swath SWOT Altimetry Observations in the Western Mediterranean Sea. *IEEE Journal of Selected Topics in Applied Earth Observations and Remote Sensing* (2019), 1–11. https://doi.org/10.1109/JSTARS.2019.2903941